Subpicosecond to Second Time-Scale Charge Carrier Kinetics in Hematite-Titania Nanocomposite Photoanodes

Sub-picosecond to Second Timescale Charge Carrier Kinetics in Hematite-Titania Nanocomposite Photoanodes

Tero-Petri Ruoko,[†] Kimmo Kaunisto,[,†] Mario Bärtsch,[‡] Juuso Pohjola,[†] Markus Niederberger,[‡] Nikolai V. Tkachenko,[†] and Helge Lemmetyinen[†]*

[†]Department of Chemistry and Bioengineering, Tampere University of Technology, P.O. Box 541, 33101 Tampere, Finland.

[‡]Laboratory for Multifunctional Materials, Department of Materials, ETH Zürich, Vladimir-Prelog-Weg 5, 8093 Zürich, Switzerland.

AUTHOR INFORMATION

Corresponding Author

*E-mail: kimmo.kaunisto@tut.fi

ABSTRACT

Water splitting with hematite is negatively affected by poor intrinsic charge transport properties. However, they can be modified by forming heterojunctions to improve charge separation. For this purpose, charge dynamics of TiO_2:α-Fe_2O_3 nanocomposite photoanodes are studied using transient absorption spectroscopy to monitor the evolution of photogenerated charge carriers as a function of applied bias voltage. The bias affects the charge carrier dynamics, leading to trapped electrons in the sub-millisecond timescale and an accumulation of holes with a lifetime of 0.4 ± 0.1 seconds. In contrast, slower electron trapping and only few long-lived holes are observed in a bare hematite photoanode. The decay of the long-lived holes is one order of magnitude faster for the composite photoanodes than previously published for doped hematite, indicative of higher catalytic efficiency. These results illustrate the advantages of using composite materials to overcome poor charge carrier dynamics, leading to a 30-fold enhancement in photocurrent.

TOC GRAPHIC

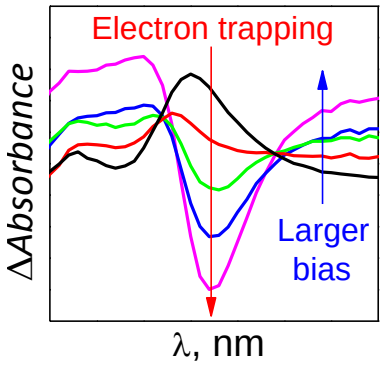

The Sun is the largest source of energy available; however, no efficient methods of storing solar power exist. Artificial photosynthesis has the potential to convert sunlight into chemical fuels that can be stored and transported over long distances, eliminating the problem of intermittent local energy production with photovoltaics. Photoelectrochemical (PEC) water reduction can be used to produce hydrogen as a renewable fuel. Ever since the discovery of PEC water splitting,[1,2] metal oxide semiconductors, such as α-Fe_2O_3 (hematite), TiO_2 (titania), and WO_3, have been preferred photoanode materials due to their abundance, non-toxicity, and thermodynamic stability.[3–8] Hematite has been especially regarded as one of the most promising photoanode materials ever since it was first used for water oxidation by Hardee and Bard.[9] Hematite has numerous desirable properties as a photoanode material: a near optimal band gap of ~2.2 eV leading to a theoretical solar-to-hydrogen efficiency of 12.9 %,[10] high chemical stability, natural abundance, and low production costs.[4,5]

However, the highest achieved solar-to-hydrogen efficiency of hematite is currently only 34 % of the theoretical limit[11] due to several factors: (i) a flat band potential too low for water reduction, (ii) a high overpotential required to oxidize water, (iii) poor electron mobility, and (iv) a small hole diffusion length of 2–20 nm.[12–15] Fast charge carrier recombination due to the poor electron mobility and the small hole diffusion length can be solved by using very thin hematite films. However, the relatively low absorption coefficient of hematite leads to a long light penetration depth. Thus, thick films are needed for complete light absorption, with many electron-hole pairs formed far from the semiconductor-electrolyte interface with no opportunity to take part in the water oxidation reaction.

To surpass these intrinsic shortcomings of hematite, two separate approaches were used to increase the photocurrent efficiency. Hematite samples were prepared from amorphous iron oxide

nanoparticles on fluorine doped tin oxide (FTO) substrates to yield mesoporous films. This effectively minimizes the distance that an electron-hole pair must diffuse to reach the semiconductor-electrolyte interface to take part in the oxidation reaction. A drawback of this approach is that the mesoporous structure increases the distance that photoexcited electrons must travel to reach the conducting substrate, while the poor electron mobility remains unchanged. However, the incorporation of titanium into hematite has been shown to increase both electron mobility and concentration, while reducing the charge carrier recombination rate.[16–20] The optimal Ti concentration has been observed to range from 1 to 10 molar percent.[20] Thus, mixed hematite-titania (0–20 molar-% Ti at 5 % intervals) films were prepared from a nanoparticle co-dispersion[21] to simultaneously minimize the distance that holes must diffuse to the electrolyte interface and increase the electron mobility. The sizes of the iron oxide and anatase nanoparticles were approximately 3 and 4 nm before deposition, respectively, yielding 250 ± 50 nm thick mesoporous nanocomposite electrodes after annealing with an average particle diameter of approximately 40–50 nm regardless of the amount of incorporated titania. A scanning electron microscope (SEM) image of the mesoporous hematite structure is presented in Figure S1. The titania forms mainly a shell-like mixed-phase pseudobrookite-iron titanate (Fe_2TiO_5) layer on top of the larger hematite nanoparticles, as observed by a possible U-shaped titanium shell layer with X-ray photoelectron spectroscopy (XPS) and the existence of titanium mainly in the surface of hematite particles with high-resolution transmission electron microscopy (HR-TEM) combined with electron energy loss spectroscopy (EELS).[21] The solubility level of titania in hematite was determined to be between 15–20 %, due to the formation of segregated distributions of hematite and titania with 20 % incorporation of TiO_2.[21] The 15 molar-% TiO_2 hematite-titania photoanode was selected as the representative nanocomposite film since it provided the highest photocurrent efficiency with

respect to sample absorption (Figures S2–S4), showing a 30-fold increase in the photocurrent at 1.23 V vs. the reversible hydrogen electrode (RHE).

Transient absorption spectroscopy (TAS) in a ps–s timescale enables the investigation of the evolution of photogenerated charge carriers from initial recombination to participation in the water oxidation reaction. Studies using TAS for hematite photoanodes with applied bias voltage have been published predominantly within the past few years.[22–30] Both bare hematite and hematite-titania photoanodes feature broad time-resolved spectra at 0 ps with a maximum at 580 nm, attributed to the absorption of photogenerated electrons and holes.[22,25,30] The transient absorption peak at 580 nm is assigned to optical transitions into localized states below the conduction band level of hematite, with a positive signal indicating the oxidation of these states.[28] The four exponential decay component spectra for the hematite-titania photoanode at 1.6 V vs. RHE are shown in Figure 1a. The ultrafast TAS decays at 580 nm are multiexponential with half-lives of 2.5–3.3 ps and 4.0–6.5 ps, respectively, as determined from the raw decay data shown in Figure 1b.

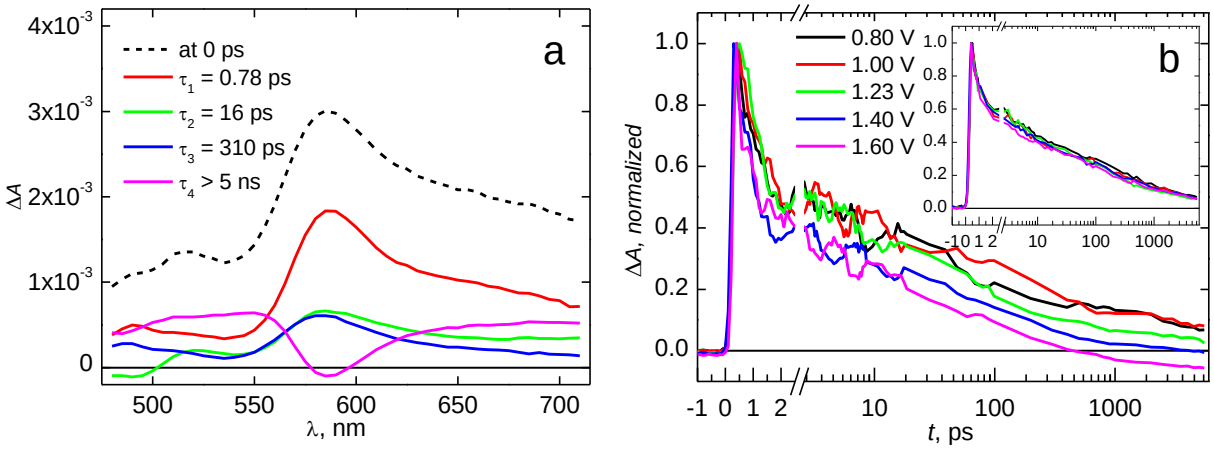

Figure 1. (a) Four-exponential decay component spectra for the hematite-titania photoanode at 1.6 V_{RHE}. (b) Normalized TAS decays at 580 nm for the bare hematite (inset) and hematite-titania (15 %) photoanodes at different bias voltages vs RHE in a ps–ns timescale.

The application of anodic bias has little effect on the TAS dynamics of the bare hematite photoanode, with the signal decaying almost completely within 6 ns except for a small residual positive absorption at 580 nm, as visible in the inset of Figure 1b and Figure S5. This decay is assigned to a primary bimolecular electron-hole recombination with no significant electron trapping on this timescale.[30] On the other hand, the anodic bias changes the ultrafast decay dynamics of the hematite-titania photoanode significantly. The positive absorption observed at 580 nm rapidly inverts into a negative bleach signal in Figures 1 and S6, assigned to electron trapping into oxidized energy states a few hundred mV below the conduction band edge.[25,28,30] Furthermore, the TAS decays are significantly prolonged at wavelengths longer and shorter than the 580 nm absorption feature with applied bias, as shown in Figures S7 and S8. This is assigned to a greatly increased amount of photogenerated holes near the valence band edge due to reduced recombination.

In the μs–s timescale the TAS decays at 580 nm for bare hematite and hematite-titania photoanodes have two distinct components, an intense negative bleach signal that inverts into a positive absorption that is observable for up to 2 s, as visible in Figures 2, S9 and S10. The decays up to 40 ms at 1.6 V_{RHE} are shown in Figure 2a, and the corresponding biexponential decay component spectra are shown in Figure 2b. The faster decay component was fitted with a small energy distribution model,[31] since band bending results in a distributed exponential lifetime for the trapped electrons. In this timescale the TAS signal amplitudes of the bare hematite film are near the instrument response limit of ~10^{-5}, as shown in Figure S11, leading to high uncertainties in the determined lifetimes and spectral features. Thus, the following discussion is limited to the hematite-titania photoanode.

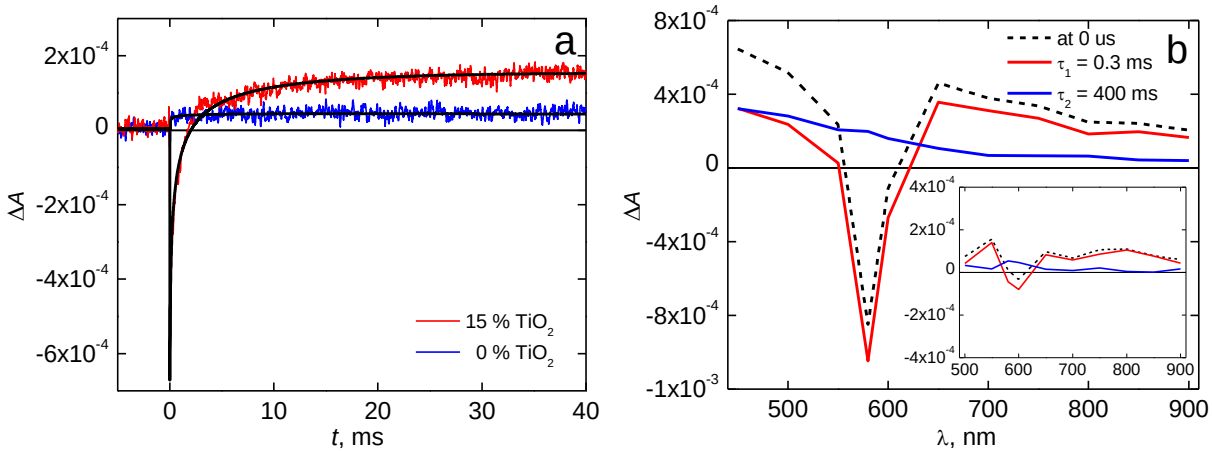

Figure 2. (a) Flash-photolysis TAS decays at 580 nm for the bare hematite and the hematite-titania (15 %) samples at 1.6 V_{RHE} in a μs–ms timescale (smoothed with a 20 point Savitzky-Golay filter). Black lines show biexponential fits to the raw data. (b) Corresponding decay component spectra for the bare hematite (inset) and hematite-titania (15 %) samples at 1.6 V_{RHE}.

The amplitude of the negative bleach signal increases with higher applied bias voltages and possesses the same spectral features observed for the longest-lived component in the ns timescale, shown in Figure 1a. This indicates a prolonged electron trapping from the ns to ms time range. The bleach signal recovers completely within 20 ms due to electron extraction from the filled energy states.[30] This is followed by a positive absorption observed throughout the probe range with lifetimes of approximately 300–400 ms at biases above the onset voltage (≥ 1 V), assigned to long-lived surface holes that can participate in the water oxidation reaction.[22,23,25]

The decay of the long-lived hole signal has been described as the rate-limiting step in the water oxidation reaction.[23] The water oxidation reaction rate for the long-lived holes was calculated using the kinetic model presented in ref. 29, where the rate constant of the long-lived hole signal decay is equal to the sum of the rate constants for water oxidation and slow back electron recombination as described by eq. 1:

$$k_{TA} = k_{\mathrm{WO}} + k_{\mathrm{BER}} = (\tau_{\mathrm{TA}})^{-1} \quad (1)$$

where k_{TA} is the decay rate of the long-lived exponential transient absorption signal, k_{WO} is the water oxidation rate, k_{BER} is the rate constant for back electron recombination and τ_{TA} is the exponential long-lived hole lifetime obtained from the two exponential global fits of raw transient absorption decays in the μs–s timescale. The water oxidation rate is presumed to be constant with respect to applied bias voltage and equal to the long-lived hole decay at the highest measured bias (1.6 V vs. RHE) due to band bending preventing electron back flow.[29] Since the exponential lifetime of the long-lived hole signal is 360 ms with negligible back electron recombination at this bias voltage, the water oxidation reaction rate for the nanocomposite electrode is calculated as $k_{\mathrm{wo}} = (\tau_{\mathrm{TA}})^{-1} = 2.78\ \mathrm{s}^{-1}$. The calculated rate constants and water oxidation yields for the long-lived holes at all measured bias voltages are presented in Table S1. A visual comparison of the rate constants at different bias voltages is presented in Figure S13a, whereas the water oxidation yield of long-lived holes is compared with the photocurrent density under simulated solar illumination in Figure S13b.

For the hematite-titania photoanode the water oxidation reaction rate is one order of magnitude higher than the previously published results for silicon doped hematite photoanodes ($k_{\mathrm{WO}} \approx 2.8\ \mathrm{s}^{-1}$ vs 0.3–0.7 s^{-1})[22,23,29] and matches the rate observed for water oxidation with titania photoanodes.[32–34] In addition, the water oxidation rate is very close to that observed for silicon doped hematite photoanodes in the presence of methanol ($k \approx 2.7\ \mathrm{s}^{-1}$)[22], a known hole scavenger. The high reaction rate obtained for the composite photoanode is indicative of increased catalytic activity due to a greatly decreased activation energy barrier.[23]

It is important to note that some of the observed signal for long-lived holes could originate from a direct excitation of possibly remaining anatase particles. However, due to the relatively low

concentration of anatase and the unfavorable band alignment for hole transport from hematite to anatase,[21] most of the long-lived signal is suggested to originate from holes in hematite. In addition, no photocurrent specific to anatase below the onset potential of hematite is observed (Figure S4), indicating that it does not directly take part in the water oxidation reaction. The observation that the incorporation of the anatase particles mainly results in the formation of a pseudobrookite-iron titanate shell over the hematite particles in these photoanodes supports the conclusion that direct excitation of anatase can only play a very minor role in the water oxidation reaction rate.[21]

Fast electron trapping to localized oxidized states near the conduction band edge of hematite has been suggested to compete with electron-hole-pair recombination, thus increasing the hole transport efficiency.[30] The longest timescale (> 5 ns) temporally resolved transient absorption spectra at different bias voltages obtained with ps–ns TAS for the bare hematite and the hematite-titania photoanodes are compared in Figure 3.

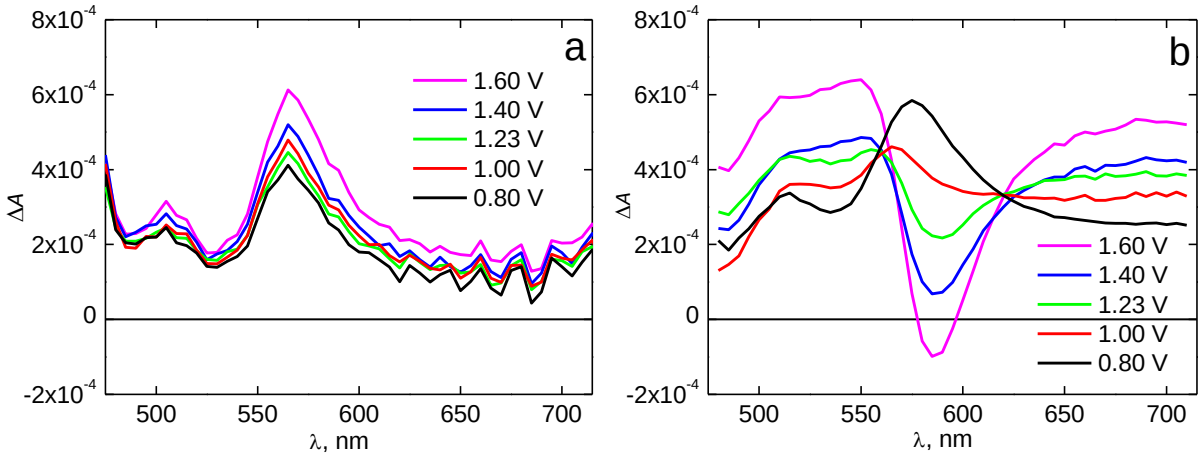

Figure 3. Longest decay component spectra (τ > 5 ns) from ps–ns TAS for the (a) bare hematite and (b) hematite-titania (15 % TiO_2) photoanodes at different bias voltages vs RHE.

In this timescale the absorption feature at 580 nm remains unchanged for the bare hematite photoanode with increased anodic bias, although a small rise in the absorbance throughout the

probe region is observed. This rise is assigned to an increased surface hole concentration due to promoted band bending at the semiconductor-electrolyte interface. On the other hand, for the hematite-titania sample the electron trapping to oxidized electron states is clearly visible at 580 nm with biases above the onset voltage. The trapping results in a greatly increased hole concentration observed at shorter and longer wavelengths than the bleach at 580 nm, and is attributed to increased charge separation due to the formation of the pseudobrookite-hematite heterojunction. It is possible that the incorporation of titania also leads to an increased density of energy states near the conduction band of hematite. This would result in a competitive trapping pathway for electrons, decreasing the electron-hole recombination rate, and thus increasing the charge carrier lifetime.[30]

The trapped electrons in the hematite-titania photoanodes have a lifetime in the ns to μs range, with the same spectral feature observed still in the millisecond timescale, as shown in Figure 4a. This is consistent with the fact that electrons trapped in oxygen vacancies in hematite cannot immediately recombine,[35] thus leading to considerably enhanced charge separation and photocurrent performance.[30] The concentration of the long-lived holes increases drastically with increased anodic voltage, as visible in Figure 4b.

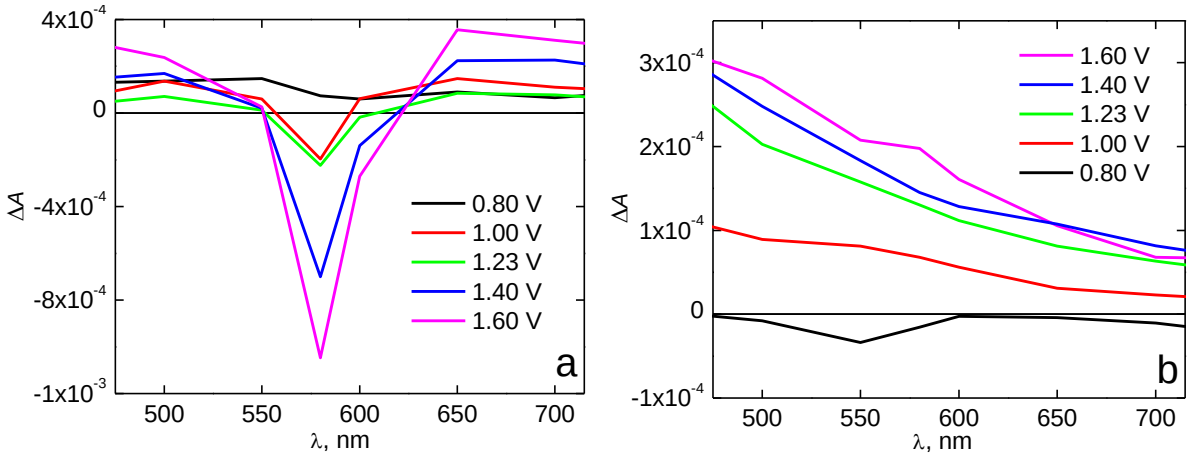

Figure 4. (a) Short- and (b) long-lived decay component spectra from μs–s TAS of the hematite-titania (15 % TiO_2) sample at different bias voltages vs RHE.

After the onset potential is reached, the hole lifetime remains stable at ~300–360 ms, as shown in Table S1 and Figure S13. This indicates a high rate for the water oxidation reaction and slow rate for the back electron recombination, with only the number of holes taking part in the reaction increasing. Only few long-lived holes are observed for the hematite-titania photoanodes at voltages below the onset potential, suggesting that the reason for high overpotentials being a prerequisite for water oxidation with hematite lies in the poor separation of holes at the semiconductor-electrolyte interface and greatly increased back electron recombination at low bias voltages. The pseudobrookite-hematite heterojunction resulting from the incorporation of titania in hematite evidently has a large effect on the charge separation process, increasing the amount of long-lived surface holes.[21] Scheme 1 illustrates the proposed mechanism with which the enhanced charge separation takes place. Since both the valence and the conduction band levels in pseudobrookite are higher than in hematite,[36] a pn-junction is created when the pseudobrookite layer forms on top of the hematite particles. This increases the charge carrier separation in the region near the junction, explaining the observed increase in the amount of long-lived holes with the nanocomposite electrode. The heterojunction also acts as a block for photogenerated electrons, retarding back electron recombination and increasing the efficiency of the photoanodes. This illustrates the importance of forming heterojunctions with nanocomposite materials, resulting in higher performances than with low level doping of hematite with titanium.

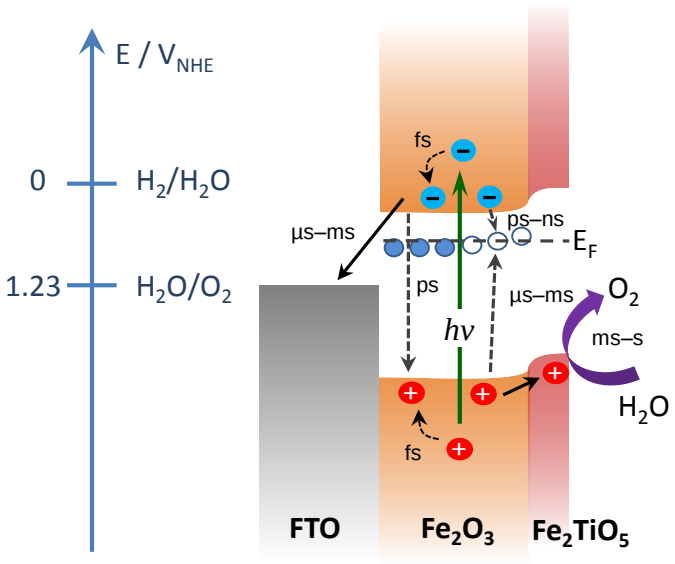

Scheme 1. Charge generation, recombination, and transfer in the nanocomposite photoelectrodes. Band bending was not incorporated in the scheme. Valence and conduction band energies are taken from ref. 36.

The results presented in this study indicate that the 30-fold increase in photocurrent performance achieved with hematite-titania composite photoanodes over bare hematite is due to two factors. First, it is shown that nanosecond timescale electron trapping into oxygen vacancies is enhanced, retarding the primary electron-hole recombination processes and hence prolonging the photogenerated hole lifetime. Second, the catalytic efficiency of the photoanodes is increased, as evidenced by room temperature kinetics for long-lived holes that are one order of magnitude faster than those previously published for hematite based photoanodes. The reaction kinetics observed match those published for methanol photo-oxidation with hematite, indicating very high catalytic performance of the photoanodes.

ASSOCIATED CONTENT

Supporting Information. Detailed experimental conditions, absorption spectra and *J-V* curves of samples, and decay component spectra at all measured timescales and applied bias voltages are presented in the Supporting Information. This material is available free of charge via the Internet at http://pubs.acs.org

AUTHOR INFORMATION

Corresponding Author

*Email: kimmo.kaunisto@tut.fi

Notes

The authors declare no competing financial interests.

ACKNOWLEDGMENT

The authors kindly acknowledge the financial support under the FP7 project SOLAROGENIX, "Visible-Light Active Metal Oxide Nano-catalysts for Sustainable Solar Hydrogen Production" (NMP4-SL-2012-310333)

REFERENCES

(1) Boddy, P. J. Oxygen Evolution on Semiconducting TiO_2. *J. Electrochem. Soc*. **1968**, *115*, 199–203.

(2) Fujishima. A.; Honda, K. Electrochemical Photolysis of Water at a Semiconductor Electrode. *Nature* **1972**, *238*, 37–38.

(3) Sartoretti, C. J.; Alexander, B. D.; Solarska, R.; Rutkowska, W. A.; Augustynski, J.; Cerny, R. Photoelectrochemical Oxidation of Water at Transparent Ferric Oxide Film Electrodes. *J. Phys. Chem. B* **2005**, *109*, 13685–13692.

(4) Sivula, K.; Le Formal, F.; Grätzel, M. Solar Water Splitting: Progress Using Hematite (α-Fe_2O_3) Photoelectrodes. *ChemSusChem* **2011**, *114,* 432–449.

(5) Sivula, K. Metal Oxide Photoelectrodes for Solar Fuel Production, Surface Traps, and Catalysis. *J. Phys. Chem. Lett.* **2013**, *4*, 1624–1633.

(6) Nowotny, J.; Bak, T.; Nowotny, M. K.; Sheppard, L. R. Titanium Dioxide for Solar-hydrogen I. Functional Properties. *Int. J. Hydrogen Energy* **2007**, *32*, 2609–2629.

(7) Santato, C.; Odziemkowski, M.; Ulmann, M.; Augustynski, J. Crystallographically Oriented Mesoporous WO_3 Films: Synthesis, Characterization, and Applications. *J. Am. Chem. Soc.* **2001**, *123*, 10639–10649.

(8) Sayama, K.; Nomura, A.; Zou, Z.; Abe, R.; Abe, Y.; Arakawa, H. Photoelectrochemical Decomposition of Water on Nanocrystalline $BiVO_4$ Film Electrodes under Visible Light. *Chem. Commun*. **2003**, 2908–2909.

(9) Hardee, K. L.; Bard, A. J. Semiconductor Electrodes V. The Application of Chemically Vapor Deposited Iron Oxide Films to Photosensitized Electrolysis. *J. Electrochem. Soc*. **1976**, *123*, 1024–1026.

(10) Murphy, A. B. Efficiency of Solar Water Splitting using Semiconductor Electrodes. *Int. J. Hydrogen Energy*, **2006**, *31*, 1999–2017.

(11) Kim, J. Y.; Magesh, G.; Youn, D. H.; Jang, J.-W-; Kubota, J.; Domen, K.; Lee, J. S. Single-Crystalline, Wormlike Hematite Photoanodes for Efficient Solar Water Splitting. *Sci. Rep.*, **2013**, *3:2681*, 1–8.(12) Dare-Edwards, M. P.; Goodenough, J. B.; Hamnett, A.; Trevellick, P. R.

Electrochemistry and Photoelectrochemistry of Iron(III) Oxide. *J. Chem. Soc., Faraday Trans. 1*, **1983**, *79*, 2027–2041.

(13) Quinn, R. K.; Nasby, R. D.; Baughman, R. J. Photoassisted Electrolysis of Water using Single Crystals of α-Fe_2O_3 Anode. *Mater. Res. Bull*. **1976**, *11*, 1011–1017.

(14) Itoh, K.; Bockris, J. O. Stacked Thin-Film Photoelectrode using Iron-Oxide. *J. Appl. Phys.* **1984**, *56*, 874–876.

(15) Kennedy, J. H.; Frese, K. W. Photooxidation of Water at α-Fe_2O_3 Electrodes. *J. Electrochem. Soc*. **1978**, *125*, 709–714.

(16) Wang, G.; Ling, Y.; Wheeler, D. A.; George, K. E. N.; Horsley, K.; Heske, C.; Zhang, J. Z.; Li, Y. Facile Synthesis of Highly Photoactive α-Fe_2O_3-Based Films for Water Oxidation. *Nano Lett*. **2011**, *11*, 3503–3509.

(17) Lian, X.; Yang, X.; Liu, S.; Xu, Y.; Jiang, C.; Chen, J.; Wang, R. Enhanced Photoelectrochemical Performance of Ti-doped Hematite Thin Films Prepared by the Sol–Gel Method. *Appl. Surf. Sci.* **2012**, *258*, 2307–2311.

(18) Zandi, O.; Klahr, B. M.; Hamann, T. W. Highly Photoactive Ti-doped α-Fe_2O_3 Thin Film Electrodes: Resurrection of the Dead Layer. *Energy Environ. Sci.* **2013**, *6*, 634–642.

(19) Kim, D. W.; Riha, S. C.; Demarco, E. J.; Martinson, A. B. F.; Farha, O. K.; Hupp, J. T. Greenlighting Photoelectrochemical Oxidation of Water by Iron Oxide. *ACS Nano* **2014**, *8*, 12199–12207.

(20) Kronawitter, C. X.; Zegkinoglou, I.; Shen, S.-H.; Liao, P.; Cho, I. S.; Zandi, O.; Liu, Y.-S.; Lashgari, K.; Westin, G.; Guo, J.-H.; et al. Titanium Incorporation into Hematite Photoelectrodes:

Theoretical Considerations and Experimental Observations. *Energy Environ. Sci.* **2014**, *7*, 3100–3121.

(21) Monllor-Satoca, D.; Bärtsch, M.; Fàbrega, C.; Genç, A.; Hilaire, S.; Andreu, T.; Arbiol, J.; Niederberger, M.; Morante, J. R. What Do you Do, Titanium? Insight into the Role of Titanium Oxide as Water Oxidation Promoter in Hematite-based Photoanodes. *Energy Environ. Sci.* Submitted.

(22) Pendlebury, S. R.; Barroso, M.; Cowan, A. J.; Sivula, K.; Tang, J.; Grätzel, M.; Klug, D. R.; Durrant, J. R. Dynamics of Photogenerated Holes in Nanocrystalline α-Fe_2O_3 Electrodes for Water Oxidation Probed by Transient Absorption Spectroscopy. *Chem. Commun.* **2011**, *47*, 716–718.

(23) Cowan, A. J.; Barnett, C. J.; Pendlebury, S. R.; Barroso, M.; Sivula, K.; Grätzel, M.; Durrant, J. R.; Klug, D. R. Activation Energies for the Rate-Limiting Step in Water Photooxidation by Nanostructured α-Fe_2O_3 and TiO_2. *J. Am. Chem. Soc.* **2011**, *133*, 10134–10140.

(24) Barroso, M.; Cowan, A. J.; Pendlebury, S. R.; Grätzel, M.; Klug, D. R.; Durrant, J. R. The Role of Cobalt Phosphate in Enhancing the Photocatalytic Activity of α-Fe_2O_3 toward Water Oxidation. *J. Am. Chem. Soc.* **2011**, *133*, 14868–14871.

(25) Barroso, M.; Mesa, C. A.; Pendlebury, S. R.; Cowan, A. J.; Hisatomi, T.; Sivula, K.; Grätzel, M.; Klug, D. R.; Durrant, J. R. Dynamics of Photogenerated Holes in Surface Modified α-Fe_2O_3 Photoanodes for Solar Water Splitting. *Proc. Natl. Acad. Sci. U.S.A.*, **2012**, *109*, 15640–15645.

(26) Pendlebury, S. R.; Cowan, A. J.; Barroso, M.; Sivula, K.; Ye, J.; Grätzel, M.; Klug, D. R.; Tang, J.; Durrant, J. R. Correlating Long-lived Photogenerated Hole Populations with

Photocurrent Densities in Hematite Water Oxidation Photoanodes. *Energy Environ. Sci.* **2012**, *5*, 6304–6312.

(27) Cowan, A. J.; Durrant, J. R. Long-lived Charge Separated States in Nanostructured Semiconductor Photoelectrodes for the Production of Solar Fuels. *Chem. Soc. Rev*. **2013**, *42*, 2281–2293.

(28) Barroso, M.; Pendlebury, S. R.; Cowan, A. J.; Durrant, J. R. Charge Carrier Trapping, Recombination and Transfer in Hematite (α-Fe_2O_3) Water Splitting Photoanodes. *Chem. Sci.* **2013**, *4*, 2724–2734.

(29) Le Formal, F.; Pendlebury, S. R.; Cornuz, M.; Tilley, S. D.; Grätzel, M.; Durrant, J. R. Back Electron-Hole Recombination in Hematite Photoanodes for Water Splitting. *J. Am. Chem. Soc.* **2014**, *136*, 2564–2574.

(30) Pendlebury, S. R.; Wang, X.; Le Formal, F.; Cornuz, M.; Kafizas, A.; Tilley, S. D.; Grätzel, M.; Durrant, J. R. Ultrafast Charge Carrier Recombination and Trapping in Hematite Photoanodes under Applied Bias. *J. Am. Chem. Soc.* **2014**, *136*, 9854–9857.

(31) Lehtivuori, H.; Efimov, A.; Lemmetyinen, H.; Tkachenko, N. V. Distributed Decay Kinetics of Charge Separated State in Solid Film. *Chem. Phys. Lett.* **2007**, *437*, 238–242.

(32) Tang, J.; Durrant, J. R.; Klug, D. R. Mechanism of Photocatalytic Water Splitting in TiO2. Reaction of Water with Photoholes, Importance of Charge Carrier Dynamics, and Evidence for Four-Hole Chemistry. *J. Am. Chem. Soc.* **2008**, *130*, 13885–13891.

(33) Cowan, A. J.; Tang, J.; Leng, W.; Durrant, J. R.; Klug, D. R. Water Splitting by Nanocrystalline TiO_2 in a Complete Photoelectrochemical Cell Exhibits Efficiencies Limited by Charge Recombination. *J. Phys. Chem. C* **2010**, *114*, 4208–4214.

(34) Tang, J.; Cowan, A. J.; Durrant, J. R.; Klug, D. R. Mechanism of O_2 Production from Water Splitting: Nature of Charge Carriers in Nitrogen Doped Nanocrystalline TiO_2 Films and Factors Limiting O_2 Production. *J. Phys. Chem. C* **2011**, *115*, 3143–3150.

(35) Rivera, R.; González, S.; Stashans, A. Microstructure and Optical Properties of α-Fe_2O_3 Containing F-centres. *Superlattice Microstruct.* **2010**, *47*, 225–231.

(36) Courtin, E.; Baldinozzi, G.; Sougrati, M. T.; Stievano, L.; Sanchez, C.; Laberty-Robert, C. New Fe_2TiO_5-Based Nanoheterostructured Mesoporous Photoanodes with Improved Visible Light Photoresponses. *J. Mater. Chem. A.* **2014**, *2*, 6567–6577.